Loss of White Matter Microstructural Integrity Is Associated with Adverse Neurological Outcome in Tuberous Sclerosis Complex

Jurriaan M. Peters, MD, Mustafa Sahin, MD, PhD, Vanessa K. Vogel-Farley, BSc, Shafali S. Jeste, MD, Charles A. Nelson, III, PhD, Matthew C. Gregas, PhD, Sanjay P. Prabhu, MBBS, Benoit Scherrer, PhD, Simon K. Warfield, PhD

Rationale and Objectives: Tuberous sclerosis complex (TSC) is a genetic neurocutaneous syndrome in which cognitive and social-behavioral outcomes for patients vary widely in an unpredictable manner. The cause of adverse neurologic outcome remains unclear. The aim of this study was to investigate the hypothesis that disordered white matter and abnormal neural connectivity are associated with adverse neurologic outcomes.

Materials and Methods: Structural and diffusion magnetic resonance imaging was carried out in 40 subjects with TSC (age range, 0.5–25 years; mean age, 7.2 years; median age, 5 years), 12 of whom had autism spectrum disorders (ASD), and in 29 age-matched controls. Tractography of the corpus callosum was used to define a three-dimensional volume of interest. Regional averages of four diffusion scalar parameters of the callosal projections were calculated for each subject. These were the average fractional anisotropy (AFA) and the average mean, radial, and axial diffusivity.

Results: Subjects with TSC had significantly lower AFA and higher average mean, radial, and axial diffusivity values compared to controls. Subjects with TSC and ASD had significantly lower AFA values compared to those without ASD and compared to controls. Subjects with TSC without ASD had similar AFA values compared to controls.

Conclusion: Diffusion tensor scalar parameters provided measures of properties of the three-dimensional callosal projections. In TSC, changes in these parameters may reflect microstructural changes in myelination, axonal integrity, or extracellular environment. Alterations in white matter microstructural properties were associated with TSC, and larger changes were associated with TSC and ASD, thus establishing a relationship between altered white matter microstructural integrity and brain function.

Key Words: Tuberous sclerosis complex; diffusion tensor imaging; corpus callosum; autism spectrum disorders; normal appearing white matter.

Tuberous sclerosis complex (TSC) is a genetic neurocutaneous syndrome with an estimated incidence of one in 6000 to 10,000. Although some patients with TSC may never show neurologic symptoms affecting their quality of life, epilepsy occurs in 80% to 90% of all patients, close to 45% of patients have mild to profound intellectual disabilities, and autism spectrum disorders (ASD) occur in up to 50% of patients (1).

The cause of neurologic deficits in patients with TSC is a key unresolved question, and neurologic outcomes remains highly variable and unpredictable. It has been hypothesized that tubers disrupt local cerebral architecture, resulting in impaired brain function. However, no robust conventional magnetic resonance imaging (MRI) measure of tubers correlates consistently with the clinical phenotype or long-term neurologic outcomes (2), and neither a high tuber load nor tubers in specific locations are necessary or sufficient to predict seizures, cognitive impairment, or autism (3).

More recently, investigators have studied the hypothesis that disordered white matter and abnormal neural circuitry contribute to neurologic symptoms in patients with TSC.

Acad Radiol 2012; 19:17–25

From the Department of Neurology (J.M.P., M.S., M.C.G.), the Department of Radiology/Computational Radiology Laboratory (J.M.P., S.P.P., B.S., S.K.W.), the Laboratories of Cognitive Neuroscience (V.K.V.-F., C.A.N.), and the Clinical Research Program (M.C.G.), Children's Hospital Boston and Harvard Medical School, 300 Longwood Avenue, Boston, MA 02115; and the Center for Autism Research and Treatment, Semel Institute, University of California, Los Angeles, Los Angeles, California (S.S.J.). Received July 8, 2011; accepted August 30, 2011. Dr Sahin is supported in part by the John Merck Fund and a Junior Investigator Award from the Children's Hospital Boston Translational Research Program. Dr Nelson is supported by grant R01 DC010290 from the National Institutes of Health (Bethesda, MD). This investigation was supported in part by grants R01 RR021885, R01 LM010033, R03 EB008680, and UL1 RR025758 from the National Institutes of Health. **Address correspondence to:** S.K.W. e-mail: simon.warfield@childrens.harvard.edu; and M.S. e-mail: mustafa.sahin@childrens.harvard.edu

doi:10.1016/j.acra.2011.08.016

Such a neural mechanism would underlie both intellectual impairment and autism and may be responsible for comorbid autism in other disorders as well (4). Support for the existence of aberrant neural circuitry can be found in TSC mouse models. The Tsc1 and Tsc2 proteins appear to be crucial for proper axon specification, guidance, and myelination (5–7). Neuron-specific Tsc1 knockout mice display diffuse cortical and subcortical hypomyelination (6). In Tsc2 heterozygous mice, investigators have found abnormally exuberant and disordered axonal projections from the retina to the lateral geniculate nucleus, suggesting defects in axon guidance (7).

Similarly, in human subjects with TSC, diffusion tensor imaging (DTI) analysis of white matter that appears normal on conventional MRI has identified abnormalities suggesting abnormal myelination and astrogliosis (8–11). Moreover, in large studies of children with idiopathic autism (autism with no known cause), DTI abnormalities of the corpus callosum have been identified (12,13).

We hypothesized that disruption of the normal development of brain function in patients with TSC is caused by alterations in the microstructural integrity of axons and myelination. Using DTI, we compared patients with TSC with healthy controls to further characterize abnormal white matter microstructure and aberrant connectivity in TSC. In addition, we hypothesized that an increase in loss of microstructural integrity in patients with TSC would lead to an increase in cognitive and social-behavioral deficits, specifically ASD. In this study, we focused on the corpus callosum, a major commissural long-distance pathway that has been well-studied in ASD as well as in TSC.

Finally, in this paper, we introduce a novel tractographic analysis method that considers all tractographic streamlines and adjusts for partial volume averaging in the calculation of DTI measures.

MATERIALS AND METHODS

Subjects

Forty patients (age range, 0.5–25 years) with established diagnoses of TSC and 29 age-matched control subjects were imaged using 3-T MRI. Control subjects underwent imaging as part of their routine care or as part of this research study. Each MRI study was reviewed by a pediatric neuroradiologist S.P.P., and all controls had normal MRI results and normal neurologic examination results. Controls did not undergo neuropsychological evaluation as part of this study. Recruitment of subjects and data acquisition were conducted using a protocol approved by the institutional review board of Children's Hospital Boston.

All patients fulfilled the clinical criteria for definite TSC, as defined by the Tuberous Sclerosis Consensus Conference (14). All patients with TSC were neurologically examined, and clinical data were obtained during office visits and from review of medical records. ASD diagnoses were based on clinical assessment by a board-certified pediatric neurologist (M.S.), using the *Diagnostic and Statistical Manual of Mental Disorders, Fourth Edition, Text Revision* (15), and in all but the three oldest subjects supported by additional testing with the Autism Diagnostic Observation Schedule (16) by experienced behavioral specialists (S.J., V.K.V.-F.).

Data Acquisition and Analysis

The MRI protocol was based on routine clinical imaging, extended with diffusion imaging. Sedation was used only in subjects undergoing clinical imaging if necessary to prevent significant motion. The imaging protocol included a T1-weighted magnetization-prepared rapid-acquisition gradient-echo sequence and a T2-weighted turbo spin-echo sequence, with diffusion imaging (17) acquired in the axial plane, using 30 images with b = 1000 s/mm2 and five images with b = 0 s/mm2 (field of view, 22 cm; slice thickness, 2.0 mm; echo time, 88 ms; repetition time, 10 seconds; matrix size, 128 × 128; number of signals acquired, 1; iPAT = 2, modified as necessary to facilitate completion of the scan if the subject was unable to remain perfectly still).

A segmentation of the intracranial cavity was created from the structural magnetic resonance image (18,19). Compensation for residual distortion and patient motion was achieved by aligning the diffusion images to the T1-weighted magnetization-prepared rapid-acquisition gradient-echo scan, with appropriate reorientation of the gradient directions (20). Tensors were estimated using robust least squares and were displayed via color coding (21).

We used a stochastic streamline tractographic algorithm that combines the speed and efficacy of deterministic decision making at each voxel with probabilistic sampling from the space of all streamlines. Potential streamlines are stochastically initialized and evaluated, starting from a seeding region of interest (ROI), such as all the white matter in the brain. Streamlines are initialized at stochastically sampled locations inside the seeding ROI and are constructed by stepping with subvoxel resolution through the tensor field. For each potential streamline, we avoid loss of connectivity due to local aberrations by incorporating a low-pass filter along the estimated pathway for conventional stopping criteria, including streamline curvature and fractional anisotropy (FA) criteria. The range of potential streamlines examined is broad in comparison to conventional deterministic streamline tracing and is formed by log-Euclidean tensor interpolation (22) at each location, with stepping direction determined by a linear combination of tensor deflection (23) and primary eigenvector orientation, with stopping based on FA and angle criteria.

Specifically, from each stochastically selected subvoxel location p^k, a new point along the streamline is identified by stepping, with a fixed step size s, in the direction v^k, determined by the primary eigenvector of the tensor estimate at p^k:

$$p^{k+1} = p^k + v^k s$$

The new point p^{k+1} is tested to ensure that it is inside the image boundary and inside the region to be considered for tractography. A mask can be used to ensure that tractography does not step through regions with no white matter. Streamline generation is terminated if points are not validated. Streamline termination criteria related to the FA and angle changes are then checked.

The trajectory FA is assessed as a linear combination of the FA of the tensor estimate and the previous trajectory FA:

$$F^{k+1} = \alpha F^k + (1-\alpha)\mathrm{FA}(D^{K+1})$$

where $\mathrm{FA}(D^{k+1})$ is the FA of the tensor D^{k+1}. The primary eigenvector of the tensor is computed, providing e^{k+1}. The angle criterion is assessed by accumulating the cosine of trajectory angle changes, θ:

$$\theta^{k+1} = \beta\theta^k + (1-\beta)\left(\sum_{j=1}^{3} e_j^{k+1} v_k^j\right)$$

The new direction of the streamline is calculated using a combination of the primary eigenvector and tensor deflection, while accounting for the previous direction of the streamline:

$$v^{k+1} \propto \gamma v^k + (1-\gamma)\left[\delta\left(D^{k+1}\right)^{\varepsilon} v^k + (1-\delta)e^{k+1}\right]$$

Propagation of each streamline was terminated if the trajectory FA fell below 0.15 or if the tract trajectory angle exceeded 30°. The trajectories were obtained using the step size parameter $s = 0.33$ mm, $\alpha = 0.5$, $\beta = 0.5$, $\gamma = 0.5$, $\delta = 0.5$, and tensor deflection power $\varepsilon = 2$.

Furthermore, as proposed by Wakana et al (24), ROIs may be specified to ensure potential streamlines meet requirements of known anatomy, by requiring streamlines to pass through certain ROIs (selection ROIs) or requiring that they do not pass through certain ROIs (exclusion ROIs). This process of stochastically sampling potential streamlines from the seeding ROI enables us to identify the streamlines that are most consistent with the diffusion tensor image, even in the presence of abnormal anatomy. Stochastic sampling is continued until a predetermined number of streamlines has been examined, and each streamline meeting all criteria is stored. A streamline density image is then constructed by counting the number of times each streamline entered a voxel and dividing by the total number of streamlines.

The streamlines identified by stochastic tractography can be used to delineate an ROI, in which the assessment of parameters of white matter microstructural integrity may be carried out. However, such an assessment can be confounded by partial volume effects, as described by Vos et al (25). When voxels associated with a fiber tract are identified, the proportion of the voxel associated with the fiber tract is important. A common strategy to select a tract-based ROI has been to threshold the streamline density to identify voxels associated with a particular white matter (26,27). Average parameters, such as FA or mean diffusivity (MD), characteristic of the region are then assessed by computing the mean value of the parameter by summing the parameter over all the voxels above the threshold and dividing by the number of voxels in the region (26,27). Vos et al (25) demonstrated that the interaction between the geometry and curvature of a white matter fascicle and the voxel grid creates a partial volume effect that confounds the analysis. We propose to avoid the confounding due to the partial volume effect by avoiding the thresholding. Instead, we use the streamline density directly to enable an appropriate weighted average of diffusion tensor parameters. In our analysis, the diffusion tensor parameters of a region are calculated on the basis of equal weighting of each of the trajectories, rather than equal weighting of each voxel. Given a streamline density image, d, and an image of a tensor scalar parameter, p, on the same discrete image lattice with voxels indexed by i, the streamline density–weighted mean, m, and variance, v, of the parameter are given by

$$m = \frac{\sum_i d_i p_i}{\sum_i d_i}, v = \frac{\sum_i d_i (p_i - m)^2}{\sum_i d_i^2}$$

The corpus callosum ROI was located by inspection of the structural MRI scans and a color-coded image of local tensor orientation and delineated interactively (Fig 1a) using previously established criteria (24). The stochastic tractography was used to identify streamlines consistent with the projections of the corpus callosum, which are illustrated in Figure 1b. Scalar measures of FA, MD, axial diffusivity, and radial diffusivity were derived from each tensor. These measures reflect properties of the underlying white matter but do not have high specificity for particular microstructural white matter changes (28). The streamlines passing through the corpus callosum ROI were used to construct a streamline density image, constructed by counting the number of times each trajectory entered a voxel and dividing by the total number of trajectories created, as illustrated in Figures 1c and 1d. To characterize the microstructural properties of the white matter of these trajectories, streamline density–weighted averages of these scalar parameter values were calculated.

This provided four scalar variables characterizing the projections of the corpus callosum in each subject, the average FA (AFA), average MD (AMD), average axial diffusivity (AAD), and average radial diffusivity (ARD). The weighted average and variance of the FA (and similarly for the other scalar parameters) in the projections of the corpus callosum were computed as

$$\mathrm{AFA} = \frac{\sum_i d_i \mathrm{FA}_i}{\sum_i d_i} \quad \mathrm{var}(\mathrm{AFA}) = \frac{\sum_i d_i (\mathrm{FA}_i - \mathrm{AFA})^2}{\sum_i d_i^2},$$

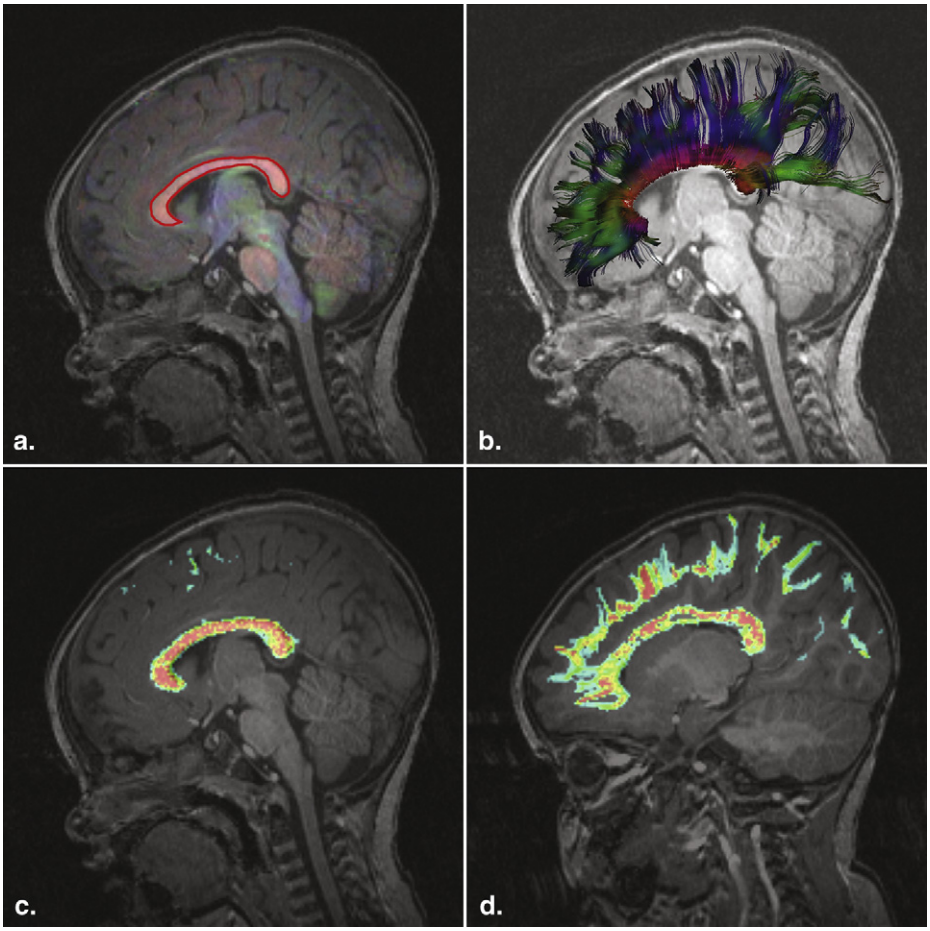

Figure 1. (a) T1-weighted image, superimposed color-coded representation of tensors, intensity proportional to the fractional anisotropy. Red for left-right, blue for superior-inferior, green for anterior-posterior. A manually drawn two-dimensional region of interest delineates the corpus callosum (CC). **(b)** Visualization of the color-coded tractography of the CC. **(c)** Streamline density–weighted image of the CC. Red (*high*) and blue (*low*) colors represent streamline density at each voxel. **(d)** Out of the midsagittal plane, the streamline density–weighted map follows the trajectories to the cortex.

where i is the index of each voxel, d_i is the streamline density at voxel i, and FA_i is the FA.

Callosal volume was estimated by thresholding the streamline density image at 5% (29), counting the number of voxels, and multiplying by the size of each voxel.

Statistical Analysis

The DTI measures were treated as response variables in a regression model with age, gender, and group status. Visual plots of the data suggest that age needed to be log transformed. This transformation was later confirmed by assessment of the value of the Akaike information criterion for the models with age log transformed and the model with age untransformed. Group status was initially defined as patients with TSC or controls. We then refined group status into three groups: controls and patients with TSC with and without ASD. All two-way and three-way interactions were considered. Interaction and main effect terms were dropped on the basis of likelihood ratio tests so that we achieved a model that accurately described the response without extraneous terms. Group and log (age) were identified as important terms. Gender was not significant after including age and group (TSC vs controls or ASD vs no ASD) in the model. The presence of group difference was determined by a likelihood ratio test. Significance tests were corrected for multiple comparisons (30), with a nominal α level of .05 and sequential model evaluation. Separate models were fit for each DTI measure. Models were validated through residual plots, Q-Q plots, and added-variable plots.

RESULTS

Patients

Forty subjects (24 male, 16 female; mean age, 7.2 years; age range, 0.5–25 years; median age, 5.0 years) underwent MRI. Only one patient had normal results on MRI. Twenty-four had clinically significant developmental delays or intellectual disabilities, and 12 had ASD (note that six patients aged < 1.5 years were not considered for formal diagnosis of ASD). Thirty patients had genetic confirmation of their clinical diagnoses with abnormalities in the Tsc1 (n = 8) and Tsc2 (n = 22) regions; in others, results were negative or testing was not performed (eg, in patients with family histories of TSC). Using Fisher's exact test, the prevalence of ASD was not significantly different in patients with Tsc1 compared to Tsc2 mutations (P = .4634), with or without global developmental delay or mental retardation (P = .2919), and with or without family histories of TSC (P = .3891). Subjects with epilepsy (n = 25) and infantile spasms

TABLE 1. *P* Values Using the Linear Regression Model with the DTI Measure as the Response and Group (Control, TSC, TSC without ASD, TSC with ASD) and Log (Age) as the Predictors

DTI Measure	Control vs TSC (All Cases)	Control vs TSC without ASD	Control vs TSC with ASD	TSC without ASD vs TSC with ASD
AMD	.000652	.022068	.000807	.128267 (NS)
ARD	.00200	.062096 (NS)	.000764	.060672 (NS)
AAD	.000876	.011224	.005148	.467143 (NS)
AFA	.0350	.8947 (NS)	.0266	.0421

AAD, average axial diffusivity; AFA, average fractional anisotropy; AMD, average mean diffusivity; ARD, average radial diffusivity; ASD, autism spectrum disorder; DTI, diffusion tensor imaging; TSC, tuberous sclerosis complex.

All four DTI measures differed significantly between controls and patients with TSC.

AFA was significantly lower in the subjects with TSC with ASD compared to those without ASD, but no difference was found between patients with TSC without ASD and controls.

(n = 11 of those 25) were more likely to have ASD (P = .0132 and P = .0256, respectively).

Twenty-nine age-matched controls (14 female, 15 male; mean age, 7.7 years; age range, 0.9–25 years; median age, 6.48 years) with normal results on MRI were included.

Diffusion Tensor Properties of Projections of the Corpus Callosum

Patients with TSC and controls. Findings and P values are presented in Table 1. Significant group differences were found, with higher AMD, AAD, and ARD values in the patients with TSC compared to controls. AFA differences between the patients with TSC and controls were again significant (P = .035) but more complex: the model fit implied that the AFA increased less with age in the TSC group than in the control group.

Patients with TSC with and without ASD and controls. Graphical displays of the linear regression model are shown in Figure 2. To summarize, significantly higher AMD, AAD, and ARD values were found in patients with TSC compared to control subjects, and a trend toward higher AMD, AAD, and ARD values was found in patients with TSC with autism compared to those without and compared to controls. Significantly lower AFA values were found in patients with TSC compared to controls (P = .035) and appeared to be nearly solely attributable to the ASD subgroup; subjects without ASD had similar AFA values as controls (P = .8947), but patients with TSC and ASD had lower AFA values than controls (P = .0266).

Callosal volume. Controls and patients with TSC without ASD were not different in estimated volume of the corpus callosum (mean, 69,717 vs 64,973 mm3; P = .2940), but controls did differ from patients with TSC with ASD (mean, 54,486 mm3; P = .00320). This difference reached significance too between patients with TSC with and without ASD (P = .0371). For all subjects and controls, the volume of the corpus callosum was inversely correlated with AMD, ARD, and AAD (Spearman's correlation = −0.80, −0.73, and −0.80, respectively, P < .000001) and correlated with AFA (Spearman's correlation = 0.40, P = .001).

DISCUSSION

Relation between White Matter Microstructure and the Development of Brain Function

Our study provides the first imaging data that identify an association between altered white matter microstructure and abnormal brain function in the TSC population. Moreover, a reduction in white matter integrity is seen in patients with worse neurodevelopmental outcomes (ie, in those who have ASD; Fig 3).

Several recent studies have reported DTI abnormalities in TSC of the normal-appearing white matter, indicating foci of microstructural abnormalities, depending on sample size and technique (8–11,31–34); summarized in Table 2. This body of data suggests that it is likely that microstructural changes are present throughout the cerebral white matter in TSC. Our study is consistent with previous literature and is the first to allow for phenotypical correlation because of its large sample size.

In TSC, several pathophysiologic substrates have been proposed for reduced FA and increased MD in the normal-appearing white matter. Changes in axonal integrity and diameter can affect axial diffusivity (35). RD values correlate with myelination in the normally developing mouse brain and in experimental dysmyelination (36). In our subjects, increased RD may represent disordered myelin sheaths but also axonal depletion or extracellular changes such as astrogliosis and giant cells (9,10). Such changes, including abnormal neuronal organization and hypomyelination, have been shown in animal models of TSC (6). Finally, lower FA may relate to disorganized (37) and poorly myelinated (38) axons. Our findings are again in accordance with animal studies, where loss of Tsc1 or Tsc2 function has detrimental effects on regulation of axonal growth, particularly neuronal polarity and axon formation (5–7).

In idiopathic autism, the white matter appears normal on conventional imaging, but the theory of "developmental disconnection" has driven research efforts in the direction of investigating connectivity on the functional and microstructural levels. In this model, disconnection relates to

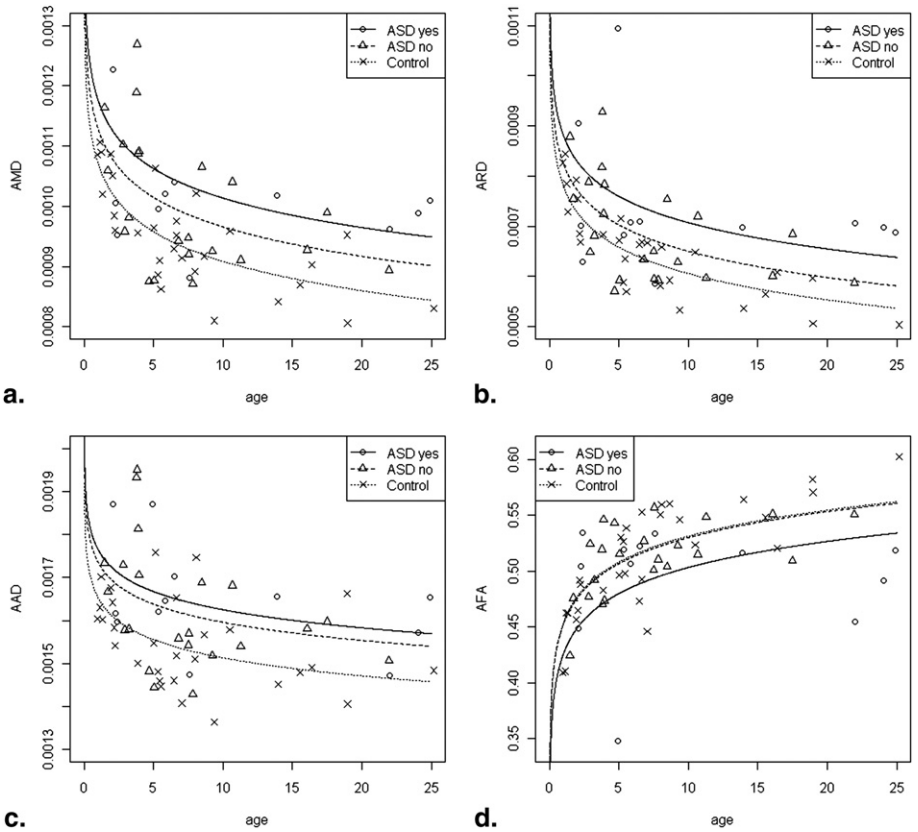

Figure 2. Graphical displays of the fit linear regression model for **(a)** average mean diffusivity (AMD), **(b)** average radial diffusivity (ARD), and **(c)** average axial diffusivity (AAD). Controls *(dotted line)* have lower AMD, ARD, and AAD than patients with tuberous sclerosis complex (TSC) with autism spectrum disorders (ASD; *solid line*), but this difference reaches significance only for AMD and AAD when controls are compared to patients with TSC without ASD *(dashed line)*. For average fractional anisotropy (AFA) **(d)**, controls and patients with TSC without ASD have highly similar values. AFA of the patients with TSC with ASD are significantly lower than controls and patients with TSC without ASD.

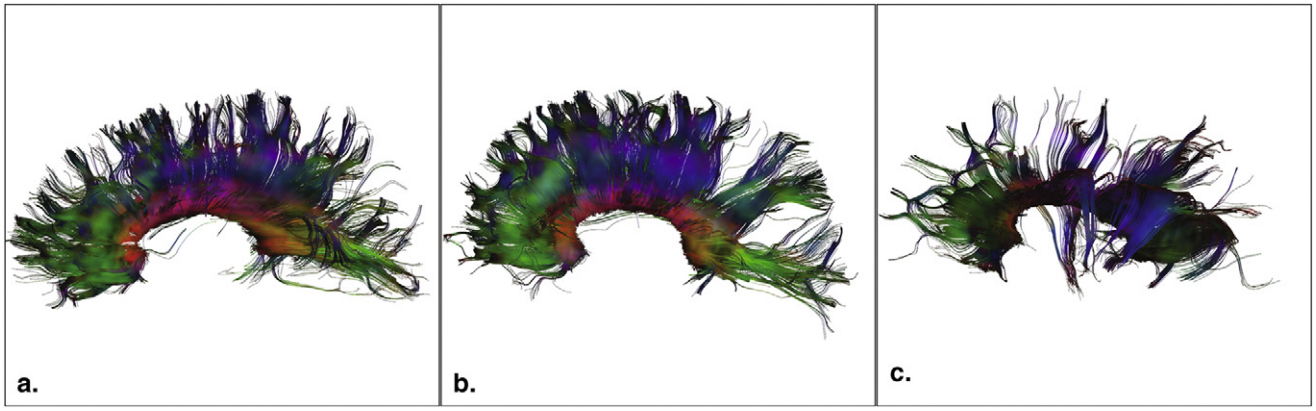

Figure 3. Illustration of projections of the corpus callosum and average fractional anisotropy (AFA) values: **(a)** a 5.3-year-old healthy control, AFA = 0.53; **(b)** a 4.7-year-old patient with tuberous sclerosis complex (TSC) but no autism spectrum disorder (ASD), AFA = 0.54; and **(c)** a 4.9-year-old patient with TSC and ASD, AFA = 0.34.

impaired corticocortical transfer of intrahemispheric and interhemispheric information, affecting the higher order processing of complex information. In patients with ASD, these processing difficulties have been found to be consistently deficient across multiple domains and across multiple modalities (12,39–41).

Within the white matter, the corpus callosum has been implicated in ASD in several lines of research, including imaging studies of callosal volume, white matter density, functional imaging of information transfer or resting state functional connectivity, and postmortem studies (12,41,42). The corpus callosum represents a major interhemispheric tract of highly coherent white matter fibers, making it especially suited for DTI to study its microstructural connectivity as a model for disconnection in autism (12), and indeed, white matter microstructural abnormalities have been identified with diffusion imaging in patients with idiopathic autism (43–45). Our DTI data confirm microstructural abnormalities of callosal white matter in patients with TSC and more prominently in the subjects with TSC with ASD, in support of the

TABLE 2. Summary of Published DTI Studies Involving NAWM in TSC

Study	n	Age (y)*	MRI	Directions	Key Findings†
Garaci et al (2004) (32)	18	20 (12–30)	1.5 T	6	MD of perilesional NAWM higher than contralateral NAWM. NAWM of frontal, occipital, and parietal regions and CSO higher MD.
Peng et al (2004) (33)	7	0.5–15	1.5 T	6	Lower FA of WM lesions associated with tubers vs contralateral NAWM. Higher MD of CR and SS. Increased $\lambda 3$ of ILF and SS.
Karadag et al 2005 (40)	7	2–20	1.5 T	6	Higher MD of tubers vs cortex of controls. Increased MD and lower FA in WM lesions and perilesional WM. No difference in MD and FA of NAWM.
Firat et al (2006) (41)	6	9 (3–15)	1.5 T	6	MD of tubers higher than NAWM. MD of NAWM not different from controls.
Makki et al (2007) (9)	6	10 (6–15)	1.5 T	6	Higher MD, lower FA in combined NAWM of genu/splenium CC, IC/EC. Greatest increase was in $\lambda 2,3$ (ie, RD).
Arulrajah et al (2009) (8)	23	12 (1–25)	1.5 T	3–18	Increased MD of frontal and pontine NAWM (in subgroup aged 8–12 y), right parietal and occipital NAWM (in subgroup aged > 12 y).
Krishnan et al (2010) (10)	10	1.5–25	3 T	35	Lower FA in splenium CC and GCT, lower AD in IC, STG and GCT, increased MD and RD in splenium CC.
Simao et al (2010) (11)	12	9 (5–16)	3 T	15	Increased MD, decreased FA, increased RD in genu and splenium CC. Increased MD in IC. DTI measures of genu and splenium CC correlate with tuber volume (not number).
This study	40	7 (0.5–25)	3 T	35	Lower FA, higher MD, RD, AD of entire CC in TSC (all) and TSC (with ASD). Lower FA of CC in TSC with ASD vs TSC without ASD. No difference in FA of CC in TSC without ASD.

AD, axial diffusivity; ASD, autism spectrum disorder; CC, corpus callosum; CR, corona radiata; CSO, centrum semiovale; DTI, diffusion tensor imaging; EC, external capsule; FA, fractional anisotropy; GCT, geniculocalcarine tract; IC, internal capsule; ILF, inferior longitudinal fasciculus; MD, mean diffusivity; MRI, magnetic resonance imaging; NAWM, normal-appearing white matter; RD, radial diffusivity; SS, sagittal striatum; STG, superior temporal gyrus; TSC, tuberous sclerosis complex; WM, white matter.

*Age is expressed as mean (range) or as range.

†Patients with TSC compared to controls unless otherwise stated.

notion that abnormal white matter microstructure is related to impaired brain development and function.

Our volume estimation data are in concordance with findings of decreased callosal volume in autism in multiple imaging studies, summarized by Anderson et al (42). In TSC, cortical malformations including tubers and neuronal migration defects affect white matter as migrational failure results in impaired neocortical development, which is followed by a deficiency in corticocortical fibers destined to be part of the corpus callosum (46,47). In a recent study of 12 patients with TSC, DTI indices of major commissural white matter also correlated with tuber load (11), suggesting more extensive malformation leading to both more tubers and decreased microstructural quality of the corpus callosum. We found significant correlations between DTI parameters and volume estimates of projections of the corpus callosum. In this interhemispheric pathway, both macrostructural and microstructural characteristics were abnormal in patients with TSC with ASD.

Streamline Density-Weighted Statistics

There are certain artifacts and pitfalls that must be taken into consideration with respect to diffusion imaging and tractography (52). Partial volume mixing and proximity of a pathway to other pathways containing many more tracts propagating in a different direction are some of the factors that introduce errors or even cause certain pathways to be missed completely. DTI tractography is consistent with known anatomy (24,49) and with the histologic appearance of fiber structure (50,51), but some fiber tracts are not identified, and spurious fiber tracts may be incorrectly detected.

Our use of streamline density weighting compensates for partial volume averaging of fiber tracts and treats each streamline in the same way. The alternative, of identifying a region on the basis of thresholding the streamline density and treating each voxel equally, fails to account for the different occupancy of voxels with many streamlines in comparison to voxels with few streamlines present. In this way, we compute the mean scalar parameter of each streamline of a structure rather than of each voxel. Thus, our use of streamline density–weighted statistics enables the analysis of the three-dimensional callosal projections while appropriately adjusting for changes in streamline density as well as spurious tracts. We propose that our calculation of streamline density–weighted averages of DTI scalar parameter values be used as a standard in the characterization of the microstructural properties of white matter fascicles.

CONCLUSIONS

Our novel method of streamline density–weighted calculation of mean DTI scalar parameters allows for the incorporation of

all white matter projections while compensating for volume averaging, resulting in average DTI measures of a white matter structure defined by tractography rather than by its voxels. Using streamline density weighting, we found a relation between alterations in white matter microstructure and neurologic outcomes in TSC.

The finding of decreased AFA and increased AAD, AMD, and ARD of the corpus callosum in the TSC population compared to controls is a new finding consistent with the previous work that has identified alterations in the white matter of patients with TSC. These pathologic findings in the corpus callosum by DTI are likely typical of alterations throughout the cerebral white matter in TSC.

The significant difference of AFA between subjects with TSC with and without ASD lends further support to the current hypothesis of long-range functional and structural disconnection in autism. Our finding of AFA differences raises the possibility of using callosal AFA as an early biomarker to predict ASD in the TSC population. Future longitudinal studies of our younger patients will provide much-needed insights in pathologic developmental changes occurring at the critical periods in ASD (41).

ACKNOWLEDGMENTS

Thanks go to Sarah Spence, MD, PhD for critical reading of the manuscript. We gratefully acknowledge the contribution of MRI scans from John Gilmore and Martin Styner, supported by grant P50 MH064065 from the National Institutes of Health. We are indebted to the children and families who have participated in this study.

REFERENCES

1. Curatolo P, Bombardieri R, Jozwiak S. Tuberous sclerosis. Lancet 2008; 372:657–668.
2. Wong V. Study of the relationship between tuberous sclerosis complex and autistic disorder. J Child Neurol 2006; 21:199–204.
3. Jansen FE, Vincken KL, Algra A, et al. Cognitive impairment in tuberous sclerosis complex is a multifactorial condition. Neurology 2008; 70: 916–923.
4. Clifford S, Dissanayake C, Bui QM, et al. Autism spectrum phenotype in males and females with fragile X full mutation and premutation. J Autism Dev Disord 2007; 37:738–747.
5. Choi YJ, Di Nardo A, Kramvis I, et al. Tuberous sclerosis complex proteins control axon formation. Genes Dev 2008; 22:2485–2495.
6. Meikle L, Talos DM, Onda H, et al. A mouse model of tuberous sclerosis: neuronal loss of Tsc1 causes dysplastic and ectopic neurons, reduced myelination, seizure activity, and limited survival. J Neurosci 2007; 27: 5546–5558.
7. Nie D, Di Nardo A, Han JM, et al. Tsc2-Rheb signaling regulates EphA-mediated axon guidance. Nat Neurosci 2010; 13:163–172.
8. Arulrajah S, Ertan G, Jordan L, et al. Magnetic resonance imaging and diffusion-weighted imaging of normal-appearing white matter in children and young adults with tuberous sclerosis complex. Neuroradiology 2009; 51:781–786.
9. Makki MI, Chugani DC, Janisse J, et al. Characteristics of abnormal diffusivity in normal-appearing white matter investigated with diffusion tensor MR imaging in tuberous sclerosis complex. AJNR Am J Neuroradiol 2007; 28:1662–1667.
10. Krishnan ML, Commowick O, Jeste SS, et al. Diffusion features of white matter in tuberous sclerosis with tractography. Pediatr Neurol 2010; 42: 101–106.
11. Simao G, Raybaud C, Chuang S, et al. Diffusion tensor imaging of commissural and projection white matter in tuberous sclerosis complex and correlation with tuber load. AJNR Am J Neuroradiol 2010; 31:1273–1277.
12. Alexander AL, Lee JE, Lazar M, et al. Diffusion tensor imaging of the corpus callosum in Autism. Neuroimage 2007; 34:61–73.
13. Keller TA, Kana RK, Just MA. A developmental study of the structural integrity of white matter in autism. Neuroreport 2007; 18:23–27.
14. Roach ES, Gomez MR, Northrup H. Tuberous sclerosis complex consensus conference: revised clinical diagnostic criteria. J Child Neurol 1998; 13:624–628.
15. American Psychiatric Association. Diagnostic and statistical manual of mental disorders. 4th ed, text rev. Arlington, VA: American Psychiatric Association; 2000.
16. Lord C, Risi S, Lambrecht L, et al. The autism diagnostic observation schedule-generic: a standard measure of social and communication deficits associated with the spectrum of autism. J Autism Dev Disord 2000; 30: 205–223.
17. Reese TG, Heid O, Weisskoff RM, et al. Reduction of eddy-current-induced distortion in diffusion MRI using a twice-refocused spin echo. Magn Reson Med 2003; 49:177–182.
18. Grau V, Mewes AU, Alcaniz M, et al. Improved watershed transform for medical image segmentation using prior information. IEEE Trans Med Imaging 2004; 23:447–458.
19. Weisenfeld NI, Warfield SK. Automatic segmentation of newborn brain MRI. Neuroimage 2009; 47:564–572.
20. Ruiz-Alzola J, Westin CF, Warfield SK, et al. Nonrigid registration of 3D tensor medical data. Med Image Anal 2002; 6:143–161.
21. Douek P, Turner R, Pekar J, et al. MR color mapping of myelin fiber orientation. J Comput Assist Tomogr 1991; 15:923–929.
22. Arsigny V, Fillard P, Pennec X, et al. Log-Euclidean metrics for fast and simple calculus on diffusion tensors. Magn Reson Med 2006; 56: 411–421.
23. Lazar M, Weinstein DM, Tsuruda JS, et al. White matter tractography using diffusion tensor deflection. Hum Brain Mapp 2003; 18:306–321.
24. Wakana S, Jiang H, Nagae-Poetscher LM, et al. Fiber tract-based atlas of human white matter anatomy. Radiology 2004; 230:77–87.
25. Vos SB, Jones DK, Viergever MA, et al. Partial volume effect as a hidden covariate in DTI analyses. Neuroimage 2011; 55:1566–1576.
26. Kubicki M, Alvarado JL, Westin CF, et al. Stochastic tractography study of Inferior Frontal Gyrus anatomical connectivity in schizophrenia. Neuroimage 2011; 55:1657–1664.
27. Powell HW, Parker GJ, Alexander DC, et al. Hemispheric asymmetries in language-related pathways: a combined functional MRI and tractography study. Neuroimage 2006; 32:388–399.
28. Basser PJ, Pierpaoli C. Microstructural and physiological features of tissues elucidated by quantitative-diffusion-tensor MRI. J Magn Reson B 1996; 111:209–219.
29. Chung HW, Chou MC, Chen CY. Principles and limitations of computational algorithms in clinical diffusion tensor MR tractography. AJNR Am J Neuroradiol 2011; 32:3–13.
30. Ge Y, Sealfon SC, Speed TP. Some step-down procedures controlling the false discovery rate under dependence. Stat Sin 2008; 18:881–904.
31. Widjaja E, Simao G, Mahmoodabadi SZ, et al. Diffusion tensor imaging identifies changes in normal-appearing white matter within the epileptogenic zone in tuberous sclerosis complex. Epilepsy Res; 89:246–253.
32. Garaci FG, Floris R, Bozzao A, et al. Increased brain apparent diffusion coefficient in tuberous sclerosis. Radiology 2004; 232:461–465.
33. Peng SS, Lee WT, Wang YH, et al. Cerebral diffusion tensor images in children with tuberous sclerosis: a preliminary report. Pediatr Radiol 2004; 34: 387–392.
34. Luat AF, Makki M, Chugani HT. Neuroimaging in tuberous sclerosis complex. Curr Opin Neurol 2007; 20:142–150.
35. Budde MD, Xie M, Cross AH, et al. Axial diffusivity is the primary correlate of axonal injury in the experimental autoimmune encephalomyelitis spinal cord: a quantitative pixelwise analysis. J Neurosci 2009; 29: 2805–2813.
36. Song SK, Yoshino J, Le TQ, et al. Demyelination increases radial diffusivity in corpus callosum of mouse brain. Neuroimage 2005; 26:132–140.
37. Beaulieu C, Allen PS. Determinants of anisotropic water diffusion in nerves. Magn Reson Med 1994; 31:394–400.
38. Gulani V, Webb AG, Duncan ID, et al. Apparent diffusion tensor measurements in myelin-deficient rat spinal cords. Magn Reson Med 2001; 45: 191–195.

39. Geschwind DH, Levitt P. Autism spectrum disorders: developmental disconnection syndromes. Curr Opin Neurobiol 2007; 17:103–111.
40. Karadag D, Mentzel HJ, Gullmar D, et al. Diffusion tensor imaging in children and adolescents with tuberous sclerosis. Pediatr Radiol 2005; 35: 980–983.
41. Firat AK, Karakas HM, Erdem G, et al. Diffusion weighted MR findings of brain involvement in tuberous sclerosis. Diagn Interv Radiol 2006; 12: 57–60.
42. Anderson JS, Druzgal TJ, Froehlich A, et al. Decreased interhemispheric functional connectivity in autism. Cereb Cortex 2011; 21:1134–1146.
43. Jou RJ, Jackowski AP, Papademetris X, et al. Diffusion tensor imaging in autism spectrum disorders: preliminary evidence of abnormal neural connectivity. Aust N Z J Psychiatry 2011; 45:153–162.
44. Lange N, Dubray MB, Lee JE, et al. Atypical diffusion tensor hemispheric asymmetry in autism. Autism Res 2010; 3:350–358.
45. Shukla DK, Keehn B, Lincoln AJ, et al. White matter compromise of callosal and subcortical fiber tracts in children with autism spectrum disorder: a diffusion tensor imaging study. J Am Acad Child Adolesc Psychiatry 2010; 49:1269–1278.
46. Volpe JJ. Neurology of the newborn. Philadelphia: Saunders, 2008.
47. Widjaja E, Blaser S, Miller E, et al. Evaluation of subcortical white matter and deep white matter tracts in malformations of cortical development. Epilepsia 2007; 48:1460–1469.
48. Le Bihan D, Poupon C, Amadon A, et al. Artifacts and pitfalls in diffusion MRI. J Magn Reson Imaging 2006; 24:478–488.
49. Zhang Y, Zhang J, Oishi K, et al. Atlas-guided tract reconstruction for automated and comprehensive examination of the white matter anatomy. Neuroimage 2010; 52:1289–1301.
50. Dauguet J, Peled S, Berezovskii V, et al. Comparison of fiber tracts derived from in-vivo DTI tractography with 3D histological neural tract tracer reconstruction on a macaque brain. Neuroimage 2007; 37:530–538.
51. Leergaard TB, White NS, de Crespigny A, et al. Quantitative histological validation of diffusion MRI fiber orientation distributions in the rat brain. PLoS One 2010; 5:e8595.